Transient fluid flow in the continuous steel-slab casting mold

Brian G. Thomas, Quan Yuan, S. Sivaramakrishnan, and S.P. Vanka
Dept. of Mechanical & Industrial Engineering
University of Illinois at Urbana-Champaign
Ph 217-333-6919; bgthomas@uiuc.edu

Abstract

Transient flow in a continuous casting mold is quantified using two recent tools for studying flow: LES (Large Eddy Simulation) calculations and PIV (Particle Image Velocimetry) measurements. The two methods produce similar results and reveal transient flow features that are very different from time-average flow pattern. Inlet swirl causes jet oscillations and complex vortex structures evolve and decay in both the upper and lower recirculation zones. These flow structures are visualized with three transient animations. In addition, inclusion particle trajectories through the flowing liquid are computed, animated, and compared successfully with measurements.

Introduction

The quality of steel produced from continuous casting is greatly affected by fluid flow phenomena in the mold region of the process. Continuous casting is used for most of the 700 million tons of steel produced in the world each year, including over 96% of steel in the U.S [1]. Even small improvements to this established process have a large impact, so it is an ideal candidate for optimization using advanced simulation.

Some of the flow phenomena involved in slab casting are illustrated in Fig. 1. Flow enters the mold through a submerged entry nozzle, which is partly constricted by a slide gate, or stopper rod that is used to control the flow rate. The complex geometry of the nozzle ports can direct the steel jets into the mold cavity at a variety of angles, turbulence levels, and swirl components. Inside the mold cavity, the flow circulates within the liquid pool contained within the curved sides of the walls of the solidifying dendrites.
The steel jets traverse the liquid pool to impinge against the narrow faces, where their superheat may cause shell-thinning breakouts [2]. The flow pattern is controlled by the forces of momentum, and possibly also with electromagnetics, or the buoyancy from introduced gas bubbles.

The molten steel from the tundish carries harmful solid inclusions like alumina. Argon gas may be injected into the nozzle to help prevent it from clogging with alumina deposits. The inclusions and gas bubbles may be transported to the top slab to be safely removed in the slag, or may be carried deep into the caster to form internal defects, such as slivers and blisters [3]. If the steel flow velocity across the top surface is too great, it may shear off some of the liquid slag layer to form another source of harmful inclusions, if they become entrapped [4, 5]. Excessive surface flow also causes transient fluctuations

and waves in the top surface level, [6] which create most surface defects at the meniscus by disrupting solidification and confusing the level control system.

If the surface flow is too slow and cold, on the other hand, the meniscus may solidify to form hooks or deep oscillation marks, and insufficiently mix the liquid slag layer. Surface quality depends on a consistent balance within the meniscus region between fluid flow, heat transfer, thermodynamics, and mechanical interactions between the solidifying steel, solid slag rim, infiltrating molten slag, liquid steel, powder layers, inclusion particles and gas bubbles. Moreover, some of the most serious quality problems occur during transients in the process, such as ladle changes and drops in meniscus level. Plant observations have found that defects are intermittent, [7] suggesting that they are related to transient flow structures.

Flow Simulation and Measurement Tools

Turbulent flow in the mold has been studied using plant measurements, water models and mathematical models. Experimental measurements on operating continuous casting machines provide direct insights into the flow near the surface [8-10]. However, they can be difficult, dangerous, expensive and limited in accuracy. Because of the nearly equal kinematic viscosities of liquid steel and water, flow in the steel caster mold region has been studied extensively using water models, which are easier to operate and visualize [4, 8, 11-16]. To quantify the velocities, Particle Image Velocimetry (PIV), [17, 18] has been recently applied to measure velocity fields in sections through water models of the continuous casting mold [8, 15, 16]. Many advanced flow computations have been applied to the continuous casting of steel, as recently reviewed [19]. Most employ time-averaged turbulence models, such as K-ε, to tackle this difficult three-dimensional problem. Recently, however, transient simulations using Large Eddy Simulation (LES) are revealing further insights. The example animation in this section compares results from both of these powerful state-of-the-art tools: PIV and LES.

Measurements and modeling were conducted on a 0.4-scale closed-bottom water model at LTV Steel [8] for the conditions given in Table 1 and Fig. 2. Figure 3 [9] shows the time-averaged flow patterns in this typical slab-casting mold with single-phase flow issuing from a bifurcated nozzle. This figure compares time-averaged velocity vector results at the centerplane between the wide faces from Large Eddy Simulation (left) and Particle Image Velocimetry (right).

Large Eddy Simulation

The first LES simulation was achieved by computational brute force: solving the three-dimensional Navier Stokes equations on a fine (128 x 184 x 64) grid of 1.5 million nodes with time steps of 0.001sec. The simulation was performed with an in-house code, LES3D, which uses the Harlow-Welch fractional step discretization on a staggered grid. The second-order central differencing is used for the convection terms and the Crank-Nicolson scheme is used for the diffusion terms. The Adams-Bashforth scheme is employed to discretize in time with second order accuracy. The implicit diffusion terms

are solved using alternate line inversion. The pressure Poisson equation is solved using a direct Fast Fourier Transform solver. No subgrid scale model was used, so this computation might be termed a course-grid DNS (direct numerical simulation). Even with efficient parallel solution methods, described elsewhere, [20] and assuming two-fold symmetry, the simulations are quite slow and take 18 CPUs per time step or 13 days (total CPU time) on an Origin 2000 for each 30s. The second LES simulation was performed using FLUENT and included a nozzle simulation for its inlet conditions. It employed a courser grid (225,000 nodes), which required the Smagorinski sub-grid scale model for turbulence. The simulation used an implicit solver (0.01s time steps) but was slower, requiring 60 days of computation for a 30s simulation.

Particle Image Velocimetry

The PIV measurements are obtained by illuminating tiny tracer particles in a planar section through the flow with two consecutive pulses of laser light. Knowing the time interval between pulses (1.5×10^{-3}s) and the distances moved by the tracer particles (from image processing), a complete instantaneous velocity field is obtained. This procedure is usually repeated every 0.2s and the results from at least 50 such exposures are averaged to obtain the time-averaged velocity field. Further details are given elsewhere [8, 21].

Transient Flow Visualizations

Both the LES model results and PIV measurements reveal the classic pair of simple recirculation zones in each half of the mold, as compared in Figure 3. In addition to this qualitative comparison, further comparisons of the time-averaged flow profile exiting the nozzle, [9] the axial velocity profile along the jet traversing the mold to impinge on the narrow face, [10] and the velocities across the top surface towards the SEN [10] reveal quantitative agreement as well. Traditional K-ε models produce similar agreement for the time average flow pattern [10].

Animation 1 (single frame in Fig. 4) reveals that this flow pattern is actually much more complex than would appear from its time-average. In the animation frames, only some of the LES velocity vectors (left) are plotted to make the plot resolutions comparable to the PIV measurements (right). Note that spurious large vectors occasionally arise in the PIV measurements, when the digital system matches together the wrong individual tracer particle images in calculating a local velocity. These errors occur in regions near the nozzle where the velocities are greatest. They could have been removed by signal filtering, but this might have contributed other bias errors. In addition to the qualitative agreement shown in the brief time intervals compared, the RMS velocity fluctuations computed with LES and measured with PIV also agree very well [20].

The recirculation regions actually contain flow structures that vary greatly with time. The jet issuing from the nozzle has a “staircase” appearance, as it swirls in and out of the centerplane. This oscillation of the jet is revealed more clearly in Animation 2 (single frame in Fig. 5). This animation is simply a closeup obtained with PIV nearer to the nozzle.

The jet oscillation effect is missing in the first LES simulation shown, owing to the neglect of the swirl component (secondary flow velocities) at the inlet. A different LES simulation, Animation 3 (single frame in Fig. 6), which included the complex swirling flow exiting the inlet, was able to capture this phenomenon.[20, 22]. This reveals the importance of the inlet swirl conditions exiting the nozzle.

The staircase structure is significant because it causes more upward bending of the jet. This is because the extra entrainment makes the jet lose its momentum faster. This in turn leads to higher top surface velocity. Lack of turbulence in the inlet leads to a "straight" jet that deflects downward upon impinging against the narrow face and results in generally lower top surface velocity. Top surface velocity is very important to the entrainment of flux and internal inclusions.

The upper and lower roll structures each evolve chaotically between a single large recirculation structure and a complex set of evolving smaller structures and vortices. Note in particular that along the top surface, fast and slow moving flow structures alternate chaotically, sometimes producing time periods with velocity much greater than the mean. This could be significant for slag entrapment. Note in the lower recirculation zone (Animation 1), that a "short circuit" flow appears in both the calculation and the measurement. The computed time scale for this "short-circuit" vortex to form, evolve and decay has the same order as the PIV measurements (7s-10s). This structure could be significant for particle motion and entrapment in the lower recirculation zone.

Particle Trajectory Visualizations

Understanding the flow pattern gives important understanding, but further computations of associated phenomena such as inclusion particle motion and entrapment are more practical. Inclusions exiting the submerged nozzle may either float to the top surface and become entrained harmlessly into the slag layer, or may be trapped in the solidifying front, leading to defects such as internal cracks and slivers in the final rolled product. Determining where these inclusions will finally end up is thus quite important. Fig. 7 shows a 100-second animation of the trajectories of 15,000 inclusion particles in a full-scale water model, computed for the conditions in Table 2.

The simulated particles were injected at the inlet over a 1.6s time interval after the turbulent flow had reached a stationary state. Lagrangian particle trajectories were calculated using a fourth-order Runge-Kutta method at each time step, assuming a vertical buoyancy force according to the density difference and a drag force for particle Reynolds numbers up to 800 .[23] The short line near the top surface is a computational "screen", which has no effect on either the flow or trajectories, other than to record particle entrapment.

The particle trajectories are animated in Fig. 7. Initially, the particles move with the jet after injection and start to impact the narrow face at about 1.6s. Next, they split into two groups and enter either the upper or lower recirculation rolls (10s). Due in part to their

buoyancy, many of the particles in the upper roll move to the top surface and are quickly and safely removed. Other particles circulate for a significant time (100s or more) before reaching the top surface to be removed. Finally, a few particles flow out of the mold bottom with the outflow and would be trapped at a deeper position, which would lead to defects in the real steel strand.

Figure 8 shows the computed trajectories of four typical particles for 100 seconds, or until they contact the top surface (top left) or exit the domain (top right). The other two particles (lower frames) are still moving. The irregular trajectories show evidence of chaotic motion and illustrate the significant effect of the turbulent flow structures on particle transport, looking in both the wideface and narrow face directions.

The simulation conditions were chosen to match full-scale water model experiments conducted at AK Steel using plastic beads chosen to approximate the behavior of 300-micron alumina inclusions in molten steel [24]. The flow field was measured with a hot-wire anemometer, which reasonably matches the model predictions as discussed elsewhere [25, 26]. Particles reaching the top surface were trapped by a screen, removed, and weighed after 10s and 100s.

Next, the computed particle fractions removed by the screen are compared with the measurements (symbols in Fig. 9). Removal is assumed when a particle touches either the top surface or the screen from above. The removal fraction of individual groups of 500 particles differed by a factor of over 1.5, due to the sensitivity of the particle trajectories to transient variations in the flow field. However the average of 15000 particles match the measurements reasonably well. The trajectory computations were also processed to compute the particle removal rate and removal fraction to the top surface (lines) in Fig. 9. The total removal rate appears to be very large (nearly 80%) in this simulation where the walls do not trap particles.

These results indicate that a large number of particles are required to study their transport (at least 2500 in this case), and that LES has the potential to accurately predict particle trajectories and removal. Its main drawback is slow computational speed, as this single simulation of 140s required 39 days on a Pentium III 750 MHz PC for 175,000 time steps. Having simulated particle motion in a water model, further work is needed to model the real steel caster, where inclusion particles may also be entrapped by the solidifying shell (corresponding to the sidewalls of the water model).

Conclusions

Fine-grid LES (large eddy simulation) models can accurately capture both the time-averaged and transient features of the flow field in continuous casting and match reasonably well with the results of PIV (particle image velocimetry) measurements. The animations obtained with these tools reveal important transient features of the flow. Top surface velocities can intermittently become much larger than their time-average values. The inlet conditions are shown to be very important, as swirl leads to a wobbling jet that affects the impingement point and top surface velocity. Complex vortex structures

evolve and decay in both the upper and lower recirculation zones. Particle trajectories depend on the turbulent motion and can be simulated reasonably using LES, provided that a large-enough number of particles are simulated over a long-enough time interval in a large-enough domain on a fine-enough grid.

Acknowledgements

The authors wish to thank the National Science Foundation (Grants #DMI-98-00274 and #DMI-01-15486) and the Continuous Casting Consortium at UIUC, for continued support of this research, FLUENT Inc., for providing the FLUENT code, and the National Center for Supercomputing Applications (NCSA) at the UIUC for computing time. Additional thanks are extended to former students H. Bai, and T. Shi for related work on the project, and P. Dauby, M. Assar, and technicians at LTV Steel for use of the PIV system and help with the measurements

References

1. I. Christmas, "Short and Medium Term Outlook for Steel Demand," Iron & Steelmaker, Vol. 26 (12), 1999, 41-44.
2. G.D. Lawson, S.C. Sander, W.H. Emling, A. Moitra, B.G. Thomas, "Prevention of Shell Thinning Breakouts Associated with Widening Width Changes," in Steelmaking Conf. Proc., Vol. 77, ISS, Warrendale, PA, (Chicago, IL), 1994, 329-336.
3. J. Herbertson, Q.L. He, P.J. Flint, R.B. Mahapatra, "Modelling of Metal Delivery to Continuous Casting Moulds," in Steelmaking Conf. Proc., Vol. 74, ISS, Warrendale, PA, (Washington, D.C.), 1991, 171-185.
4. D. Gupta and A.K. Lahiri, "A Water Model Study of the Flow Asymmetry Inside a Continuous Slab Casting Mold," Metall. Mater. Trans. B, Vol. 27B (5), 1996, 757-764.
5. W.H. Emling, T.A. Waugaman, S.L. Feldbauer, A.W. Cramb, "Subsurface Mold Slag Entrainment in Ultra-Low Carbon Steels," in Steelmaking Conf. Proc., Vol. 77, ISS, Warrendale, PA, (Chicago, IL), 1994, 371-379.
6. T. Teshima, M. Osame, K. Okimoto, Y. Nimura, "Improvements of surface property of steel at high casting speed," in Steelmaking Conf. Proc., Vol. 71, Iron & Steel Society, Warrendale, PA, 1988, 111-118.
7. J. Knoepke, M. Hubbard, J. Kelly, R. Kittridge, J. Lucas, "Pencil Blister Reduction at Inland Steel Company," in Steelmaking Conf. Proc., Vol. 77, ISS, Warrendale, PA, (Chicago, IL), 1994, 381-388.
8. M.B. Assar, P.H. Dauby and G.D. Lawson, "Opening the Black Box: PIV and MFC Measurements in a Continuous Caster Mold," in Steelmaking Conf. Proc., Vol. 83, ISS, Warrendale, PA, (Pittsburgh, PA), 2000, 397-411.

9. S. Sivaramakrishnan, H. Bai, B.G. Thomas, P. Vanka, P. Dauby, M. Assar, "Transient Flow Structures in Continuous Cast Steel," in Ironmaking Conference Proceedings, Vol. 59, ISS, Warrendale, PA, (Pittsburgh, PA), 2000, 541-557.

10. B.G. Thomas, Q. Yuan, S. Sivaramakrishnan, T. Shi, S.P. Vanka, M.B. Assar, "Comparison of Four Methods to Evaluate Fluid Velocities in a Continuous Casting Mold," ISIJ Internat., Vol. 41 (10), 2001, 1266-1276.

11. L.J. Heaslip and J. Schade, "Physical Modeling and Visualization of Liquid Steel Flow Behavior During Continuous Casting," Iron Steelmaker, Vol. 26 (1), 1999, 33-41.

12. J.Y. Lamant, M. Larrecq, A. Mouchete, Y. Codur, J. Gancarz, A. Leclercq, "Advanced Control of Mold Operation and Improved Slab Surface Quality on Sollac Continuous Casters," in Proceedings, 6th International Iron and Steel Congress, Vol. 3, Iron & Steel Inst. Japan, Tokyo, (Nagoya, Japan), 1990, 317-324.

13. T. Honeyands and J. Herbertson, "Flow Dynamics in Thin Slab Caster Moulds," Steel Research, Vol. 66 (7), 1995, 287-293.

14. D. Gupta, S. Chakraborty and A.K. Lahiri, "Asymmetry and Oscillation of the Fluid Flow Pattern in a Continuous Casting Mould: a Water Model Study," ISIJ Internat., Vol. 37 (7), 1997, 654-658.

15. D. Xu, W.K. Jones and J.W. Evans, "PIV Physical Modeling of Fluid Flow in the Mold of Continuous Casting of Steel," in Processing of Metals and Advanced Materials: Modeling, Deisgn and Properties, B.Q. Li, ed. TMS, Warrendale, PA, (San Antonio, TX), 1998, 3-14.

16. I. Lemanowicz, R. Gorissen, H.-J. Odenthal, H. Pfeifer, "Validation of CFD calculations for the submerged entry nozzle mould system using the digital particle image velocimetry," Stahl und Eisen, Vol. 120 (9), 2000, 85-93.

17. R.J. Adrian, "Particle-Image Techniques for Experimental Fluid Mechanics," Annu. Rev. Fluid Mech., Vol. 23, 1991, 261-304.

18. C.E. Willert and M. Gharib, "Digital Particle Image Velocimetry," Experiments in Fluids, Vol. 10 (4), 1991, 181-193.

19. B.G. Thomas and L. Zhang, "Mathematical Modeling of Fluid Flow in Continuous Casting: a Review," ISIJ Internat., Vol. 41 (10), 2001, 1185-1197.

20. Q. Yuan, S. Sivaramakrishnan, S.P. Vanka, B.G. Thomas, "Large Eddy Simulations of Turbulent Flow Structures in Continuous Casting of Steel," Metall. Mater. Trans., 2001, submitted July 8, 2001.

21. H. Bai and B.G. Thomas, "Turbulent Flow of Liquid Steel and Argon Bubbles in Slide-Gate Tundish Nozzles, Part I, Model Development and Validation," Metall. Mater. Trans. B, Vol. 32B (2), 2001, 253-267.

22. Q. Yuan, personal communication, University of Illinois, 2001.

23. L. Shiller and A. Naumann, "Uber die grundlegenden Berechungen bei der Schwerkraftaufbereitung," Ver. Deut. Ing., Vol. 77, 1933, 318.

24. R.C. Sussman, M. Burns, X. Huang, B.G. Thomas, "Inclusion Particle Behavior in a Continuous Slab Casting Mold," in 10th Process Technology Conference Proc., Vol. 10, Iron and Steel Society, Warrendale, PA, (Toronto, Canada, April 5-8, 1992), 1992, 291-304.

25. B.G. Thomas, X. Huang and R.C. Sussman, "Simulation of Argon Gas Flow Effects in a Continuous Slab Caster," Metall. Trans. B, Vol. 25B (4), 1994, 527-547.

26. Q. Yuan, S.P. Vanka and B.G. Thomas, "Large Eddy Simulations of Turbulent Flow and Inclusion Transport in Continuous Casting of Steel," 2nd International Symposium on Turbulent and Shear Flow Phenomena, June 27 - 29, 2001, Royal Institute of Technology (KTH), Stockholm, Sweden, Vol. 2, 2001, 519-522.

Table 1 0.4-Scale-model simulation and experimental conditions

Dimensions/Condition	**Value**
Slide-gate orientation	90^o
Slide-gate opening, linear fraction	52%
SEN bore diameter	32mm
SEN submergence depth	77 ± 3mm
Port Height × Width	32mm × 31mm
Port thickness	11mm
Port angle, lower edge	15^o down
Port angle, upper edge	40^o down
Bottom well recess depth	4.8mm
Water model height	950mm
Water model width	735mm
Water model thickness	80 mm ± 15 mm
Inlet volumetric flow rate through each port	3.53×10^{-4} m^3/s
Averaged inlet jet angle at port	30^o
Liquid density	1000 kg/m^3
Liquid material viscosity	0.001 Pa-s
Gas injection	0%

Table 2. Full-scale water model & particle simulations.

Nozzle port size /Inlet port size (x × y) (m)	0.051 × 0.056
Submergence depth (m)	0.150
Nozzle angle	25^o
Inlet jet angle	25^o
Mold /Domain height (m)	2.152
Mold /Domain width (m)	1.83
Mold /Domain thickness (m)	0.238

Average inlet flow rate (m^3/s)	0.00344
Average inlet speed (m/s)	1.69
Fluid density (kg/m^3)	1000
Casting speed (m/s)	0.0152
Fluid kinematic viscosity (m2/s)	1.0×10^{-6}
Particle inclusion size (mm)	2 – 3 (3.8 model)
Particle inclusion density (kg/m^3)	988
Corresponding alumina inclusion diameter in steel caster (μm)	300

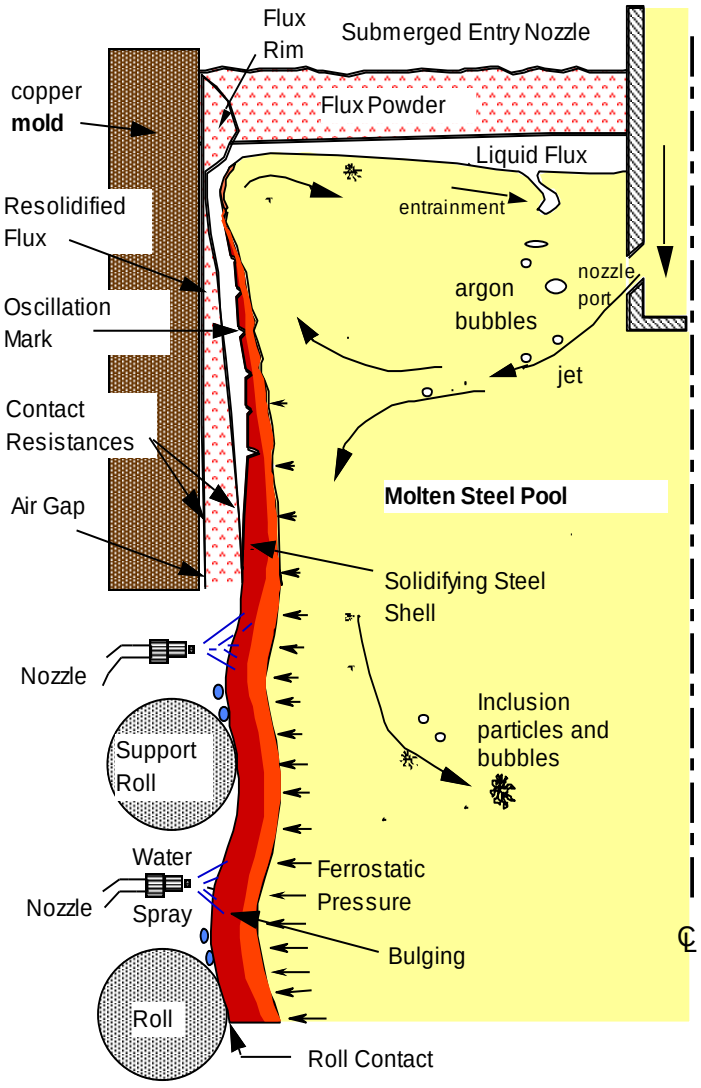

Fig. 1: Schematic of phenomena in the mold region of a steel slab caster

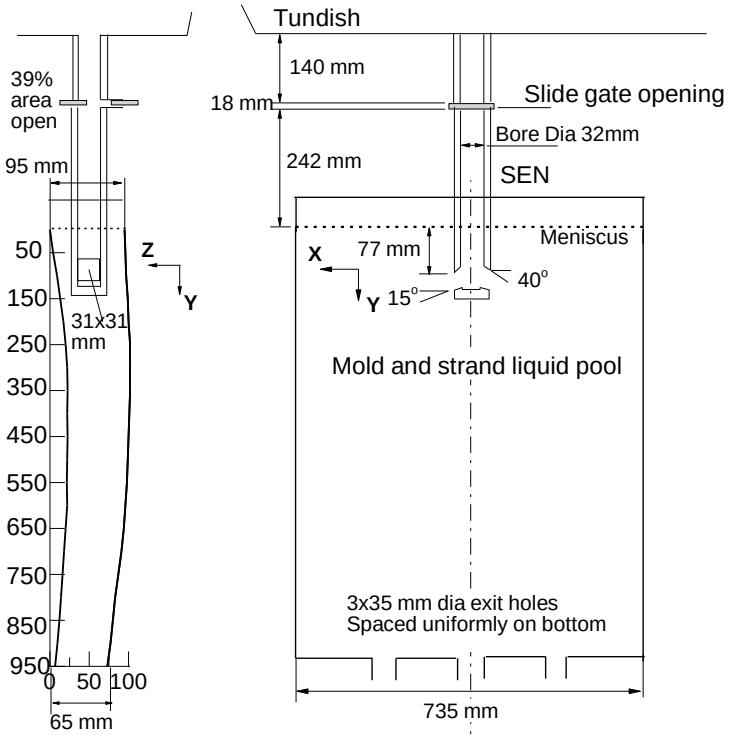

Figure 2: Schematic of the 0.4-scale water model.

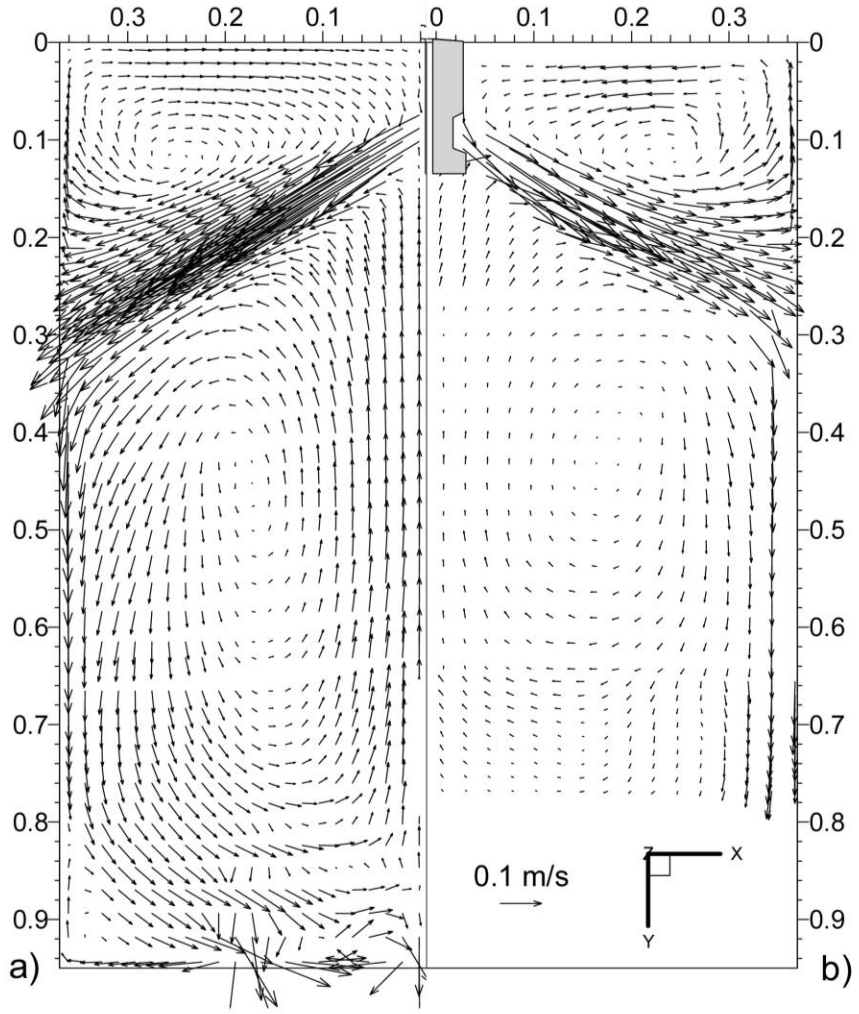

Fig. 3 Time average velocity vector plot of (a) LES simulation & (b) PIV measurement

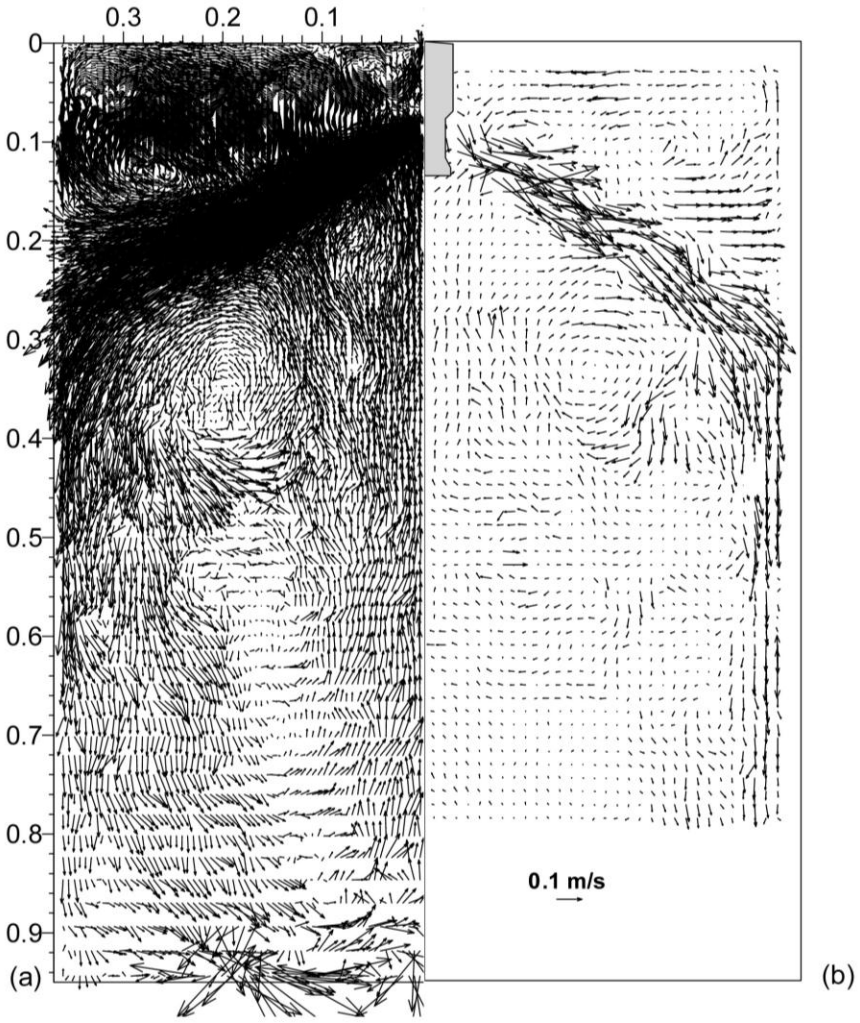

Fig. 4: Instantaneous velocity vectors in the mold from
(a) LES simulation & (b) PIV measurement
(Click on this single frame to view Animation 1)

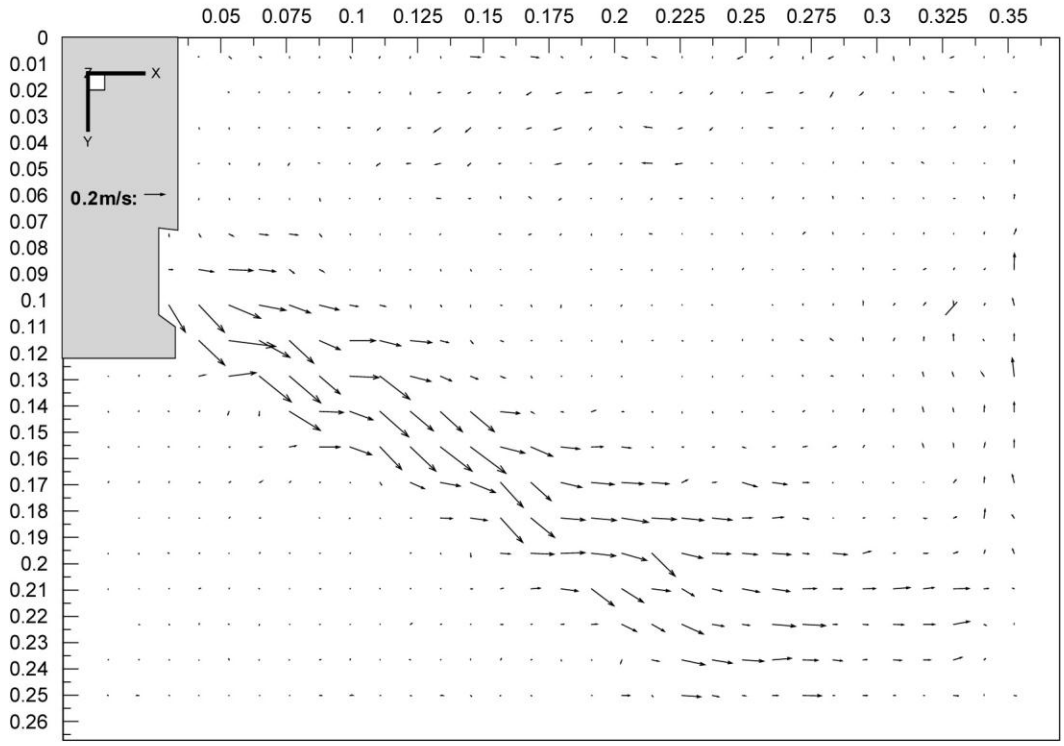

Fig. 5: PIV measurements near nozzle (Click on this single frame to view Animation 2)

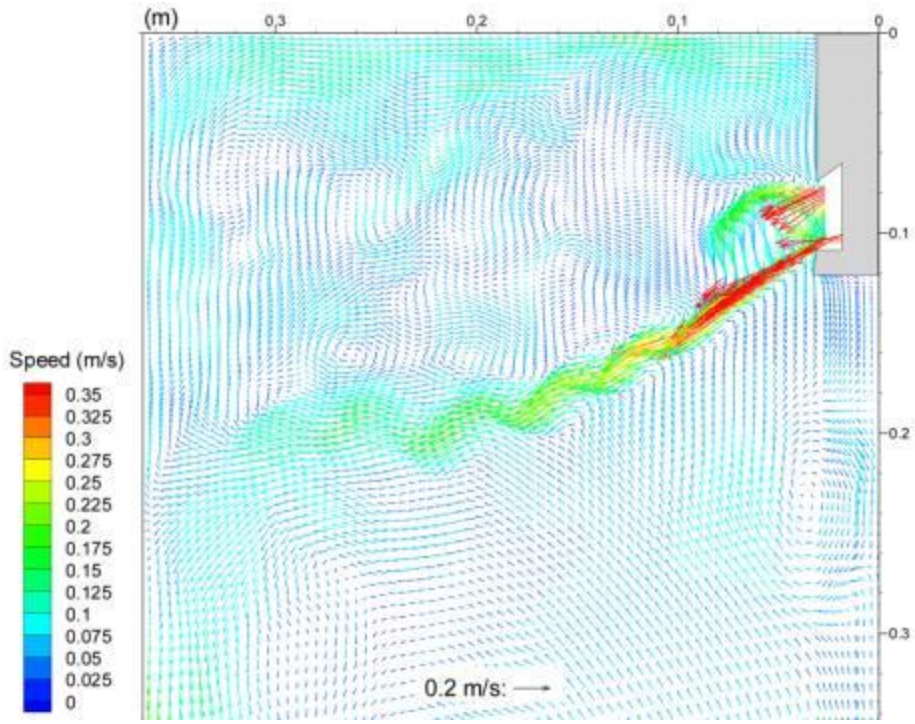

Fig. 6: LES simulation of flow near the nozzle, which includes inlet conditions from a simulation of flow in the nozzle (Click on this single frame to view Animation 3)

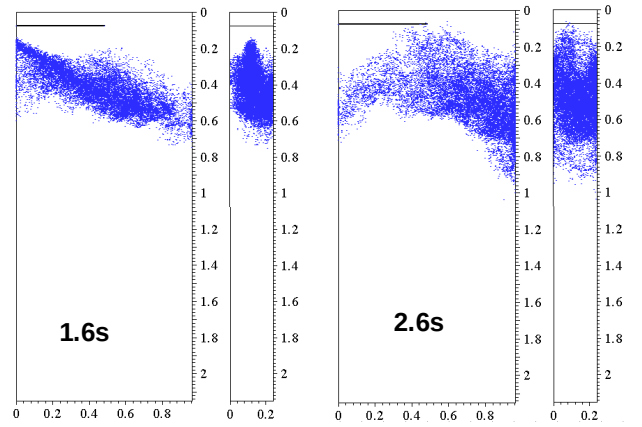

Figure 7: Distribution of 15000 particles. (Click to view Animation 4)

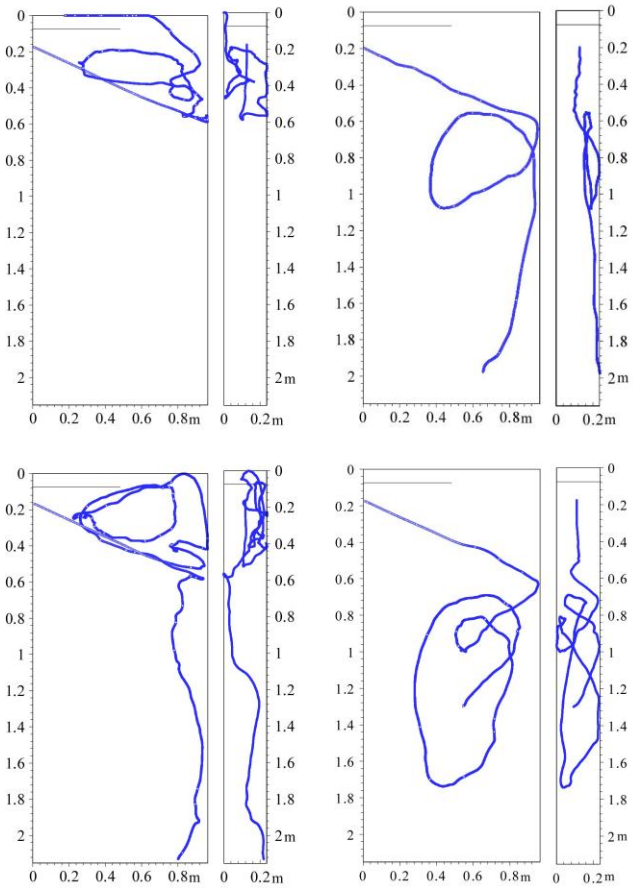

Figure 8: Four typical particle trajectory computations.

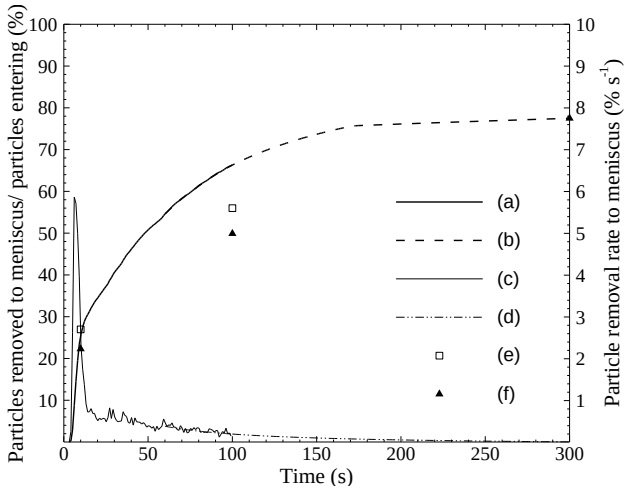

Figure 9: Particle removal to the top surface in full-scale water model:
(a) particles removed to top surface (simulated); (b) particles removed to top surface;
(c) particle removal rate to top surface; (d) particle removal rate to top surface;
(e) particles removed by screen (LES); (f) particles removed by screen (experiment)